Compressive Sensing Based 3D SAR Imaging with Multi-PRF Baselines

Liu, D.; Boufounos, P.T.

Abstract

In this paper, we fundamentally re-examine 3D SAR imaging and propose a CS-based approach aiming to reduce the data collection cost and increase the elevation resolution. In particular, our approach significantly reduces the number of baselines required to acquire the scene of interest, as well as the pulsing rate in each baseline. The baselines are collected using multiple passes of a single or multiple SAR platforms such that their elevations are randomly distributed in the available elevation space. Each baseline uses a fixed pulse repetition frequency (PRF) which can be different from the PRFs used in other baselines. Using the collected multi-baseline data in its entirety we generate a high resolution 3D reflectivity map, using a CS-based iterative imaging algorithm. Our simulation results demonstrate that the proposed method can improve elevation resolution significantly by fusing data from multiple platforms due to the very large virtual elevation aperture even with a small number of baselines.

COMPRESSIVE SENSING BASED 3D SAR IMAGING WITH MULTI-PRF BASELINES

Dehong Liu, Petros T. Boufounos

Mitsubishi Electric Research Laboratories, {*liudh,petrosb*}@merl.com

ABSTRACT

In this paper, we fundamentally re-examine 3D SAR imaging and propose a CS-based approach aiming to reduce the data collection cost and increase the elevation resolution. In particular, our approach significantly reduces the number of baselines required to acquire the scene of interest, as well as the pulsing rate in each baseline. The baselines are collected using multiple passes of a single or multiple SAR platforms such that their elevations are randomly distributed in the available elevation space. Each baseline uses a fixed pulse repetition frequency (PRF) which can be different from the PRFs used in other baselines. Using the collected multi-baseline data in its entirety we generate a high resolution 3D reflectivity map, using a CS-based iterative imaging algorithm. Our simulation results demonstrate that the proposed method can improve elevation resolution significantly by fusing data from multiple platforms due to the very large virtual elevation aperture even with a small number of baselines.

Index Terms— SAR imaging, 3D imaging, compressive sensing, high resolution

1. INTRODUCTION

Synthetic Aperture Radar (SAR) systems are high-resolution radar imaging systems that exploit the trajectory of a moving platform over the scene of interest to synthesize a large virtual aperture. Using a single pass of the moving platform, SAR systems are capable of imaging the 2-dimensional (2D) range-azimuth reflectivity of an area of interest without any elevation resolution. However, the 3-dimensional (3D) structure of the illuminated area, such as terrain features, is not preserved. The 2D image is essentially a projection of the 3D reflectivity into the 2D range-azimuth imaging plane.

This projection may cause several artifacts. For example, layover artifacts are caused when several terrain patches with different elevation angles are mapped in the same range-azimuth resolution cell [1]. In addition, certain areas might not be visible to the SAR system because a tall structure is in the illumination path, causing shadowing artifacts. In general, these artifacts can not be resolved by a single pass even using interferometric SAR techniques [2].

In recent years, 3D imaging has been realized with the launch of the TerraSAR-X [3] and the COSMO-Skymed satellites [4]. These systems exploit stacks of complex-valued SAR images from multiple passes, collected at different baselines and at different time, to form 3D images that capture the 3D location and motion of scattering objects [5]. The addition of the third (elevation) dimension enables the separation of multiple scatterers along elevation even if they are present in the same range-azimuth cell.

However, the state of the art in 3D imagery exhibits several trade-offs. First, in order to acquire multiple baselines, the platform needs to perform several passes over the area of interest. This makes data collection time consuming and very expensive. Second, the limited number of passes possible in practice with modern SAR sensors produce a small elevation aperture, also known as a tight orbital tube. Thus, the resulting elevation resolution is much lower compared to that of range and azimuth. Although the elevation resolution can be improved using compressive sensing (CS) based approaches [6], it is still not comparable to the range and azimuth resolution.

In this paper, we fundamentally re-examine 3D SAR imaging and propose a CS-based imaging approach aiming to reduce the total amount of raw data and increasing the elevation resolution. The multiple baselines are not restricted to the collection of a single platform, but multiple platforms. In particular, we assume we have multi-baseline SAR data obtained from an area of interest. Each baseline uses a fixed pulse repetition frequency (PRF) which could be different from the PRFs used in other baselines. The elevation of each baseline is randomly distributed in the available elevation space. Therefore, these baselines provide flexibility for data collection. For example, they can be multiple passes of a single SAR platform or from different SAR platforms. Assuming all the baselines are parallel and aligned to each other, we consider the multi-baseline data in its entirety to generate a high resolution 3D reflectivity map, using a CS-based iterative imaging algorithm. This work extends our earlier advances on 2D SAR imaging [7–10] to the third dimension.

Compared to earlier work on 3D tomographic SAR imaging and CS-based SAR imaging [5, 6, 11], our approach includes new contributions that provide several advantages. In particular, using our CS-based method, we are able to generate 3D reflectivity using only a very small number of baselines, thus reducing the time and cost of data collection. Moreover, by jointly processing data with different PRFs, we are able to fuse data not only from multiple passes of a single SAR platform, but also from multiple radar platforms. Although the platform flexibility may introduce alignment issues, making the SAR imaging algorithm more complicated, it provides a much larger virtual elevation aperture which significantly improves elevation resolution. Thus, we propose a novel CS-based iterative imaging method to handle multi-baseline multi-PRF data and generate high resolution 3D images even with a small number of baselines. Finally, we provide an accurate near-field range migration algorithm that generalizes far-field based 3D SAR imaging [11]. Our method, which is similar to the development in [12] for MIMO radar, is applicable for general 3D imaging using multi-pass observations, including airborne and spaceborne SAR systems.

The near-field ω–k imaging algorithm is described in the next section. Section 3 demonstrates how this algorithm can be used in conjunction with CS-based reconstruction to perform 3D imaging with limited observations. Section 4 presents experimental results that validate our approach and Sec. 5 concludes.

2. THREE-DIMENSIONAL ω–k IMAGING

A multi-baseline SAR system images a 3D ground reflectivity using a 2D planar monostatic virtual array comprised of multiple SAR platform trajectories, also referred to as baselines, shown in Fig. 1(a).

We assume that all SAR platforms operate in spotlight mode, illuminating the same area of interest. For simplicity—although not a critical assumption—we further assume that all platforms use the same pulse shape for illumination, denoted using $p(t)$ with frequency spectrum denoted using $P(\omega)$, and equal to

$$P(\omega) = \int p(t)e^{-j\omega t}dt, \qquad (1)$$

where $\omega = 2\pi f$ represents the angular frequency.

For a monostatic virtual array, the received echo reflected by the ground due to pulse $p(t)$ emitted at location (u, v, w) is

$$s(t, u, v, w) = \int_x \int_y \int_z \frac{1}{4\pi r^2} f(x, y, z)p\left(t - \frac{2r}{c}\right)dxdydz, \qquad (2)$$

where $f(x, y, z)$ is the ground reflectivity at (x, y, z) and

$$r = \sqrt{(x-u)^2 + (y-v)^2 + (z-w)^2}. \qquad (3)$$

The 4D (1D temporal plus 3D spatial) Fourier transform of the received echo can be expressed in the ω–k space as

$$S(\omega, k_u, k_v, k_w) =$$
$$\int_t \int_u \int_v \int_w s(t, u, v, w)e^{-j\omega t - jk_u u - jk_v v - jk_w w}dtdudvdw. \quad (4)$$

Using the method of stationary phase [13], (4) evaluates to

$$\begin{aligned} &S(\omega, k_u, k_v, k_w) \\ =\ & P(\omega)\frac{j}{4k}\int_x \int_y \int_z \frac{1}{x}f(x, y, z)e^{-jk_x x - jk_y y - jk_z z}dxdydz \\ =\ & P(\omega)\frac{j}{4k}\mathcal{F}_{3D}\left(\frac{1}{x}f(x, y, z)\right), \end{aligned} \qquad (5)$$

where

$$k_y = k_v,\ k_z = k_w,\ k_x = \sqrt{4k^2 - k_v^2 - k_w^2},\ k = \omega/c, \qquad (6)$$

c is the speed of light, and $\mathcal{F}_{3D}$ denotes the 3D Fourier transform.

The forward acquisition process, described in (5), models the data acquisition as a function of the ground reflectivity in the ω–k space. Using (5) and the ground reflectivity, the radar echo can be efficiently computed using the fast Fourier transform computations. It is also clear from (5) that the reflectivity map $f(x, y, z)$ can be expressed as the inverse Fourier transform of the collected SAR raw data. The corresponding inverse process, i.e., the reconstruction of the 3-D reflectivity, can be approximated by

$$\begin{aligned} &f(x, y, z) \\ =\ & x\int_{dk_x}\int_{dk_y}\int_{dk_z} -j4kS(\omega, k_u, k_v, k_w)P^*(\omega) \\ & e^{jk_x x + jk_y y + jk_z z}dk_x dk_y dk_z \\ =\ & x\mathcal{F}_{3D}^{-1}\left(-j4kS(\omega, k_u, k_v, k_w)P^*(\omega)\right). \end{aligned} \qquad (7)$$

Thus, the 3D image of the ground reflectivity can be efficiently recovered using the 3D inverse Fourier transform in the ω–k space. Note that to use (7) for reconstruction, the data acquired over (ω, k_u, k_v, k_w) first need to be weighted and rearranged into a 3D data format over (k_x, k_y, k_z) according to the dispersion relation defined in (6) using a 3D Stolt mapping, as described, e.g., in [12].
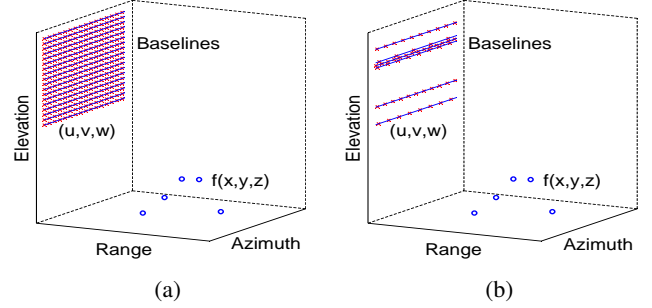

Fig. 1. (a) Schematic of 3D SAR imaging using 2D virtual array, (b) Schematic of multi-baseline multi-PRF 3D SAR imaging

3. CS-BASED 3D IMAGING

In general, when reconstructing the image using the baseline configuration of Fig. 1(a) and the reconstruction in (7), obtaining high elevation resolution requires a large vertical aperture and a corresponding large number of baselines to be collected at a sufficiently high PRF. Thus, high elevation resolution is often too expensive; practical systems typically have much lower elevation resolution.

Instead, our approach, described in Fig. 1(b) is to randomly select a subset of the baselines and to obtain data only from those selected ones, possibly using a different PRF on each. This approach significantly reduces the data acquisition burden. Since the resulting system is underdetermined, this approach requires a CS-based algorithm to recover the scene.

To better describe our CS-based 3D imaging algorithm, we compactly denote the forward process in (5) as a linear transformation

$$\mathbf{s} = \mathbf{\Phi f}, \qquad (8)$$

where $\mathbf{s}$ is the vector of the received signal (echo), $\mathbf{\Phi}$ represents the forward process and $\mathbf{f}$ is the vector of the 3D ground reflectivity.

The echoes acquired from the proposed system are essentially sub-sampled from the whole 2D virtual aperture observations according to the baseline elevations and PRFs. We denote the subsampling operator using $\mathbf{M}$. Thus, the acquired echoes are equal to

$$\mathbf{u} = \mathbf{Ms} = \mathbf{M\Phi f} = \mathbf{\Psi f}. \qquad (9)$$

To reconstruct 3D reflectivity map $\mathbf{f}$ we use an algorithm similar to [9], which decomposes $\mathbf{f}$ into a sparse component $\mathbf{f}_s$ and a dense residual $\mathbf{f}_r$. The sparse component $\mathbf{f}_s$ is estimated using standard CS-based methods:

$$\widehat{\mathbf{f}}_s = \arg\min_{\mathbf{f}} \|\mathbf{u} - \mathbf{\Psi f}\|_2^2 \text{ s.t. } \|\mathbf{f}\|_0 < T. \qquad (10)$$

The residual due to the dense component can be computed using the sparse estimate, i.e., $\widehat{\mathbf{u}}_r = \mathbf{u} - \mathbf{\Psi}\widehat{\mathbf{f}}_s$. The dense component can be estimated using least squares:

$$\widehat{\mathbf{f}}_r = \mathbf{\Psi}^\dagger(\mathbf{u} - \mathbf{\Psi}\widehat{\mathbf{f}}_s). \qquad (11)$$

The final image is the sum of the two estimates, (10) and (11).

The algorithm shown in Fig. 2 provides an efficient implementation of this approach. First a residual vector is initialized from the measurements, $\mathbf{u}_r^{(0)} = \mathbf{u}$, with $\widehat{\mathbf{f}}_s^{(0)} = \mathbf{0}$. Each iteration, k, uses the residual $\mathbf{u}_r^{(k-1)}$ to estimate the so-far unexplained signal $\widetilde{\mathbf{f}}^{(k)}$. A threshold $\tau^{(k)}$ separating the large reflectors is computed as

1. Initialize $0 < \alpha < 1$, $\widehat{\mathbf{f}}_s^{(0)} = \mathbf{0}$, $\mathbf{u}_r^{(0)} = \mathbf{u}$,

2. FOR $k = 1 : K$

$$
\begin{aligned}
\tilde{\mathbf{f}}^{(k)} &= \boldsymbol{\Psi}^\dagger \mathbf{u}_r^{(k-1)} \\
\tau^{(k)} &= \max(|\tilde{\mathbf{f}}^{(k)}|) \cdot \alpha \cdot \operatorname{sign}(K - k) \\
\mathbf{d}^{(k)} &= \mathcal{H}_{\tau^{(k)}}(\tilde{\mathbf{f}}^{(k)}) \\
\tilde{\mathbf{u}}^{(k)} &= \boldsymbol{\Psi} \mathbf{d}^{(k)} \\
\beta^{(k)} &= \frac{< \tilde{\mathbf{u}}^{(k)}, \mathbf{u}_r^{(k-1)} >}{< \tilde{\mathbf{u}}^{(k)}, \tilde{\mathbf{u}}^{(k)} >} \\
\mathbf{u}_r^{(k)} &= \mathbf{u}_r^{(k-1)} - \beta^{(k)} \tilde{\mathbf{u}}^{(k)} \\
\widehat{\mathbf{f}}_s^{(k)} &= \widehat{\mathbf{f}}_s^{(k-1)} + \beta^{(k)} \mathbf{d}^{(k)}
\end{aligned}
$$

END

3. Output

Image: $\widehat{\mathbf{f}} = \widehat{\mathbf{f}}_s^{(K)}$

Fig. 2. Reconstruction algorithm

a fraction of the largest in magnitude component. After hard thresholding, $\mathcal{H}_{\tau^{(k)}}\left(\tilde{\mathbf{f}}^{(k)}\right)$, i.e., setting all components less than $\tau^{(k)}$ in magnitude to zero, the strongest reflectors are kept in $\mathbf{d}^{(k)}$. This estimate is scaled, using $\beta^{(k)}$, to capture most of the residual energy in $\mathbf{u}_r^{(k-1)}$, and added to the overall signal estimate from the previous iteration $\widehat{\mathbf{f}}_s^{(k-1)}$ to produce the current signal estimate $\widehat{\mathbf{f}}_s^{(k)}$. The residual $\mathbf{u}_r^{(k-1)}$ is updated and the algorithm iterates. At the Kth iteration, with the threshold τ^K being set to zero, the remaining residual is used to estimate the dense part of the final image using the least squares method. The final image $\widehat{\mathbf{f}}$ combines the sparse part of previous $(K-1)$ iterations and the dense part of the Kth iteration.

This algorithm is inspired by STOMP [14], but differs in estimating the sparse signal in each iteration. Specifically, we do not compute the psudo-inverse of a subset of $\boldsymbol{\Psi}$. Instead, similarly to the matching pursuit (MP) [15], we use the signal value after thresholding, scaled by $\beta^{(k)}$, as an estimate of the sparse signal. Although we do not provide a theoretical analysis with reconstruction guarantees, we found that this heuristic choice provides a good trade-off between speed and accuracy compared to classical CS algorithms. We also found that a good choice for the thresholding parameter α in our algorithm is $\alpha > 0.5$.

4. EXPERIMENTS

To verify our approach, we simulated the SAR acquisition using (5) followed by reconstruction using both conventional imaging methods and the proposed approach. For simplicity, we consider a 2D virtual array located in the azimuth-elevation plane, i.e. $u = 0$.

Our first experiment images point scatterers placed in a 3D space. We collect a total of 70 baselines, randomly distributed along the elevation direction. These baselines are selected from 281 possible baselines, uniformly spaced along the elevation, as shown in Fig. 1(b). Raw SAR data are collected from each baseline with a fixed PRF. However, for each baseline, the corresponding PRF is randomly selected. Specifically, starting from a reference PRF, all baselines have PRFs downsampled by a random integer amount. In other words, each PRF is a fraction of the reference PRF, with the downsampling rate randomly selected from the set $\{2,3,4,5\}$. We
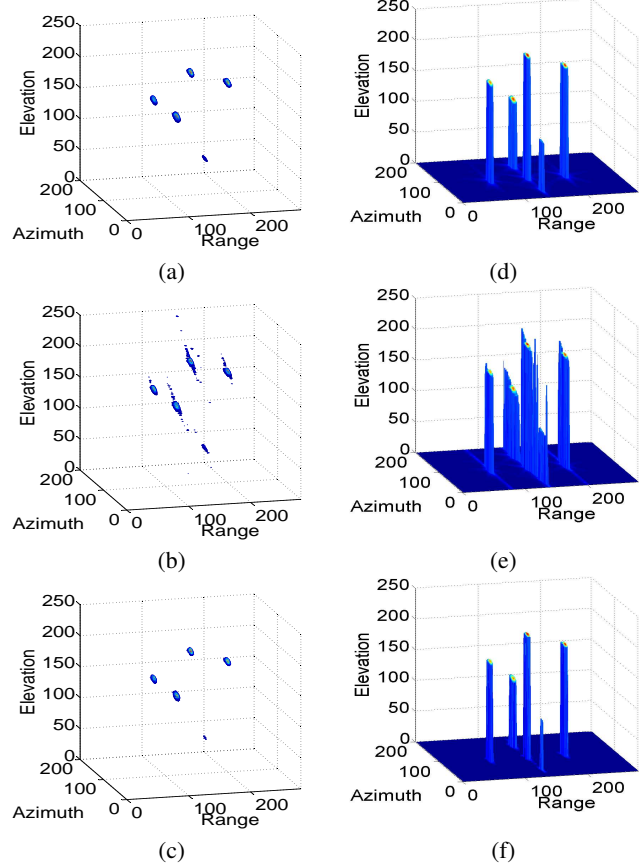

Fig. 3. (a) Reconstruction using data from 281 baselines at high PRF, (b) Conventional reconstruction with 70 baselines each with different, reduced PRF, and (c) CS-based reconstruction using the same limited data as (b). (d)-(f) are 3D surface plots of (a)-(c), respectively, that clearly show the height of the recovered scatterers.

assume the data are perfectly aligned.

We compare three different approaches: (a) full data collection from all 281 possible baselines using the reference PRF for all baselines and conventional reconstruction, (b) reduced data collection using 70 baselines, each with different PRF, and conventional reconstruction, and (c) reduced data collection, as in (b), and our CS-based reconstruction approach. For conventional 3D imaging with reduced data collection, we use the ω–k imaging algorithm in (7) by upsampling the data and filling the missing data with zeros. This algorithm produces a fast beamforming reconstruction from the acquired data, implementing the inverse of the acquisition operator. For CS-based imaging, we use the iterative algorithm in Fig. 2 that exploits the sparsity of the scene to fill-in the missing data, and then perform fast ω–k imaging.

The results are shown in Fig. 3. In the left column, from top to bottom, we plot the reconstructed reflectivities, as follows: (a) assuming a full data collection, (b) using limited data collection and conventional imaging methods, and (c) using limited data collection and CS-based reconstruction. The color intensity represents the intensity of the recovered reflectivity. In the right column, plots (d)-(f) show the same results as (a)-(c) respectively using surface plots to more clearly demonstrate the height of the recovered scatterers.

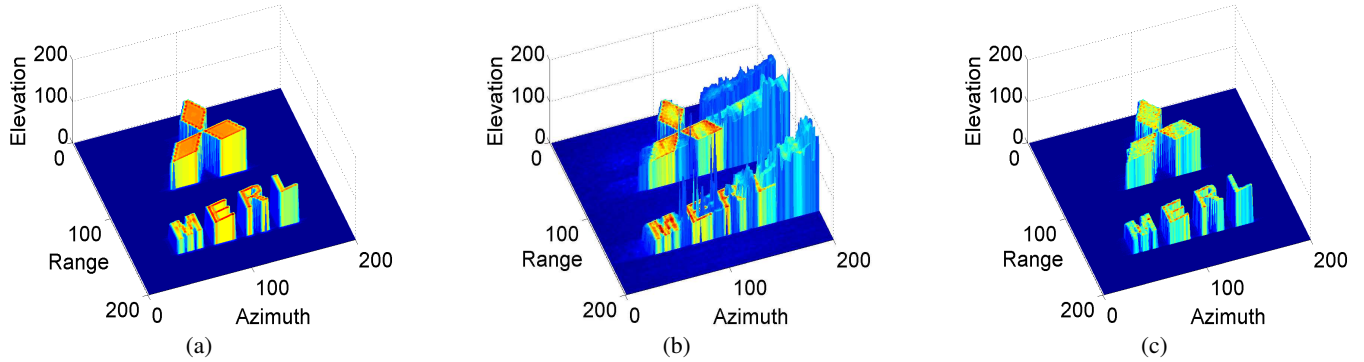As evident in the figure, imaging using the full data collection

Fig. 4. (a) Reconstruction using data from 281 baselines at high PRF, (b) Conventional reconstruction with 28 baselines each with different, reduced PRF, and (c) CS-based reconstruction using the same limited data as (b).

clearly retrieves point scatterers in the 3D space. The reconstruction does, in fact, correspond to the ground truth. However, with limited the data collection, conventional algorithms produce degraded images that exhibit low resolution in both azimuth and elevation. Our CS-based approach significantly improves the reconstruction, despite the limited available data. CS recovery is very close to conventional imaging using the full data cube, i.e., the ground truth.

Our second experiment images a more complicated object using even fewer baselines. In particular, we use a total of 28 baselines, each with a down-sampled PRF, similar to the first experiment, out of a total of 281 parallel baselines sampled at the reference PRF that comprise the full data cube.

We plot the imaging results in Fig. 4, where (a) assumes a full data collection, (b) uses limited data collection and conventional reconstruction, and (c) uses 28 baseline data collection and CS-based reconstruction. The color intensity represents the recovered reflectivity strength. As evident in the figure, CS-based reconstruction significantly improves imaging quality and retrieves the objects in the 3D space. Our reconstruction takes about 4 minutes per iteration on a $200 \times 200 \times 200$ 3D map using Matlab on a 3.6GHz Intel Xeon CPU, and requires less than 50 iterations to converge.

5. CONCLUSION

We propose a 3D SAR imaging method by fusing multi-baseline multi-PRF SAR data from multiple radar platforms using compressive sensing technique. Imaging results on point scatters and artificial objects with simulated data demonstrate that our method can recover the 3D structure of the area of interest using a small number of baselines at different PRFs. Our method provides high elevation resolution with significantly reduced data collection cost.

6. REFERENCES

[1] F. Gini, F. Lombardini, and M. Montanari, "Layover solution in multibaseline SAR interferometry," *IEEE Trans. Antennas and Propagation*, vol. 38(4), pp. 1344–1356, Oct 2002.

[2] P. Berardino, G. Fornaro, R. Lanari, and E. Sansosti, "A new algorithm for surface deformation monitoring based on small baseline differential SAR interferograms," *IEEE Trans. Geoscience and Remote Sensing*, vol. 40(11), pp. 2375–2383, Nov 2002.

[3] DLR-(German Aerospace Center), "TerraSAR-X," available at http://terrasar-x.dlr.de.

[4] ASI-(Italian Aerospace Center), "COSMO-SkyMed," available at http://www.asi.it/en/activity/earth_observation/cosmoskymed.

[5] G. Fornaro, F. Serafino, and F. Soldovieri, "Three-dimensional focusing with multipass SAR data," *IEEE Trans. Geoscience and Remote Sensing*, vol. 41(3), pp. 507–517, March 2003.

[6] X. X. Zhu and R. Bamler, "Tomographic SAR inversion by L_1-norm regularization - the compressive sensing approach," *IEEE Trans. Geoscience and Remote Sensing*, vol. 48(10), pp. 3839–3846, Oct 2010.

[7] D. Liu and P. T. Boufounos, "High resolution SAR imaging using random pulse timing," in *IEEE International Geoscience and Remote Sensing Symposium (IGARSS)*, 2011.

[8] D. Liu and P. T. Boufounos, "Random steerable arrays for synthetic aperture imaging," in *IEEE International Conference on Acoustics Speech and Signal Processing(ICASSP)*, 2013.

[9] D. Liu and P. T. Boufounos, "Synthetic aperture imaging using a randomly steered spotlight," in *IEEE International Geoscience and Remote Sensing Symposium (IGARSS)*, Australia, 2013.

[10] D. Liu and P. T. Boufounos, "High resolution scan mode sar using compressive sensing," in *Proc. Asia-Pacific Conference on Synthetic Aperture Radar (APSAR)*, Tsukuba, Japan, September 23-27 2013.

[11] J. M. Lopez-Sanchez and J. Fortuny-Guasch, "3-D imaging using range migration techniques," *IEEE Trans. Antennas and Propagation*, vol. 48(5), pp. 728–737, May 2000.

[12] X. Zhuge and A. G. Yarovoy, "Three-dimensional near-field MIMO array imaging using range migration techniques," *IEEE Trans. Image Processing*, vol. 21(6), pp. 3026–3033, June 2012.

[13] M. Born and E. Wolf, *Principles of optics*, Cambridge University press, 1999.

[14] D.L. Donoho, Y. Tsaig, I. Drori, and J.-L. Starck, "Sparse solution of underdetermined systems of linear equations by stagewide orthogonal matching pursuit," *IEEE Trans. Information Theory*, Februray 2012.

[15] S. Mallat and Z. Zhang, "Matching pursuit with time-frequency dictionaries," *IEEE Trans. Signal Process.*, vol. 41(12), Dec. 1993.